

Accuracy of Segment-Anything Model (SAM) in Medical Image Segmentation Tasks

Sheng He, Rina Bao, Jingpeng Li, P. Ellen Grant, Yangming Ou

Abstract— The segment-anything model (SAM), was introduced as a fundamental model for segmenting images. It was trained using over 1 billion masks from 11 million natural images. The model can perform zero-shot segmentation of images by using various prompts such as masks, boxes, and points. In this report, we explored (1) the accuracy of SAM on 12 public medical image segmentation datasets which cover various organs (brain, breast, chest, lung, skin, liver, bowel, pancreas, and prostate), image modalities (2D X-ray, histology, endoscopy, and 3D MRI and CT), and health conditions (normal, lesioned). (2) if the computer vision foundational segmentation model SAM can provide promising research directions for medical image segmentation. We found that SAM without re-training on medical images do not perform as accurately as U-Net or other deep learning models trained on medical images.

Index Terms—Segment anything model, Medical Image Segmentation, Deep Learning, U-Net

1 INTRODUCTION

MEDICAL image segmentation is a foundational problem aiming to automatically segment the target regions (lesions/organs) in an input image. Deep learning models trained on a large number of labeled images have achieved promising accuracy in various images/tasks [1], [2], [3], [4]. However, manually creating the ground-truth for training deep learning models is tedious work for human experts.

Recently studies about big models show successful zero-shot generalization for language processing (such as Chat-GPT) and image segmentation (such as Segment-anything SAM) [5]. In this technical report, we evaluate the zero-shot generalization of SAM on 12 different medical datasets. Our purpose is to show whether the big AI models trained on natural images can be generalized to various medical images. Fig. 1 shows the framework of the proposed method. We evaluated the SAM model on segmenting medical images collected from 11 different organs, scanned by 6 different types of imaging modalities, and compared with 5 different state-of-the-art deep learning segmentation networks that are commonly used for medical image segmentation tasks.

2 METHODS

2.1 Segmentation networks for comparison

We compared 5 different variations of state-of-the-art segmentation networks, including (1) pure U-Net based models, such as U-Net [1], U-Net++ [3], (2) attention based models, such as Attention U-Net [2], and (3) Transformer based models, such as UCTransNet [6], Trans U-Net [7]. There models are trained on each dataset with the same training configures for all models on all 12 datasets.

2.2 Review of SAM

In the computer vision domain, the Segment Anything Model (SAM) introduces a novel model, dataset, and task for image segmentation, which can be used for zero-shot transfer learning to new image distributions and tasks. The SAM model is built upon the arguably largest segmentation dataset so far, comprising over 1 billion masks on 11 million licensed and privacy-respecting natural images. It is designed to foster research into foundational models for computer vision. The model is efficient and promptable, enabling it to achieve impressive zero-shot performance that is often comparable to or better than fully supervised results in natural image segmentation. The promptable design of the SAM model allows for transfer learning to new tasks and image distributions, which can be used to develop and improve models for image segmentation. SAM has been evaluated on 23 datasets covering a broad range of domains.

2.3 Applying SAM in Medical Image Segmentation

2.3.1 Datasets

We collected 12 different public available datasets for medical image segmentation. (1) **ACDC** is from the Automated Cardiac Diagnosis Challenge [8] with the purpose of cardiac MRI (CMR) assessment. (2) **BraTS** is from 2020 Multimodal Brain Tumor Segmentation Challenge [9], [10], [11] with the purpose of segmenting brain tumor (including the peritumoral edema and tumor core) segmentation. (3) **BUID** is from Ultrasound & Breast Ultrasound Images Dataset [12] with the purpose of breast cancer segmentation. (4) **CIR** [13] consists of 956 CT images on segmented lung nodules from two public datasets. (5) **Kvasir** is from Kvasir-Seg [14] which consists of 1000 polyp images. (6) **Pancreas** [15], [16] consists of 285 CT scans with the purpose of pancreatic parenchyma and mass segmentation. (7) **Prostate** is from a Multi-site Dataset [17] which consists 116 prostate T2-weighted MRI from three different sites. (8) **ISIC** [18], [19] consists of dermoscopy images for skin lesion segmentation. (9) **LA** [20] is the dataset for automatic atrial segmentation for the left

• S.He, R.Bao, J.Li, E.Grant, Y.Ou are with the Boston Children's Hospital and Harvard Medical School, 300 Longwood Ave., Boston, MA, USA

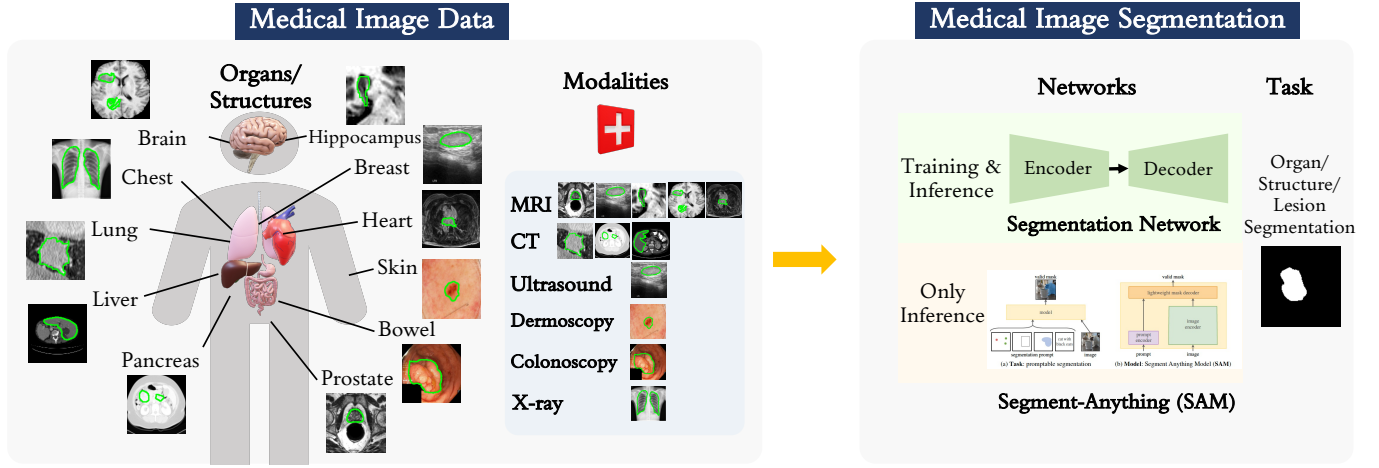


Figure 1: The framework of the proposed method. Different medical images are collected from 11 different organs and 6 different modalities. We compared two typical models for medical image segmentation: state-of-the-art segmentation networks trained on medical images and SAM trained on more than 1 million natural images.

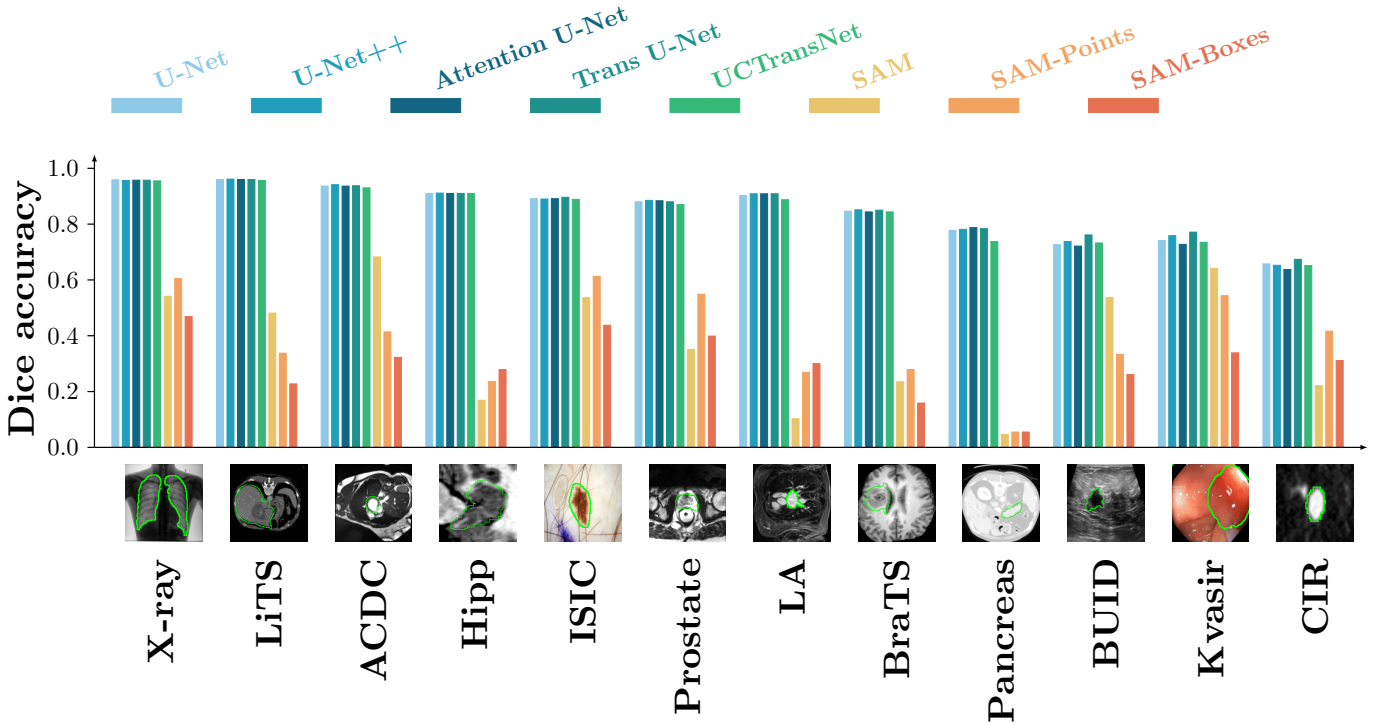


Figure 2: Dice accuracies on 12 medical image segmentation datasets. U-net, U-net++, Attention U-Net, Trans U-Net, UCTransNet were cross-validated in each medical image datasets. The SAM, SAM-Points and SAM-Boxes algorithms were applied directly on those 12 medical image datasets.

atrial (LA) on Gadolinium-enhanced cardiac magnetic resonance imaging (GE-MRI). (10) **LiTS** [21] is the image dataset containing primary and secondary liver tumors on computed tomography (CT) volumes. (11) **Hippocampus** [16] is the MRI dataset of the hippocampus proper and parts of the subiculum. (12) **Chest X-ray** [22] contains the chest X-ray images for lung segmentation.

2.3.2 Experimental Setting

We evaluated the SAM model with three settings: auto-prompt, single-point prompt, and bounding-box prompt. (I) auto-prompt setting (SAM): SAM model will sample single-point input prompts in a grid over the input image and select the high-quality masks with non-maximal suppression. All parameters are set to the default values. When multiple masks were obtained, We chose the most overlapped mask with the medical image ground-truth and used it as the prediction. (II) single-point prompt setting

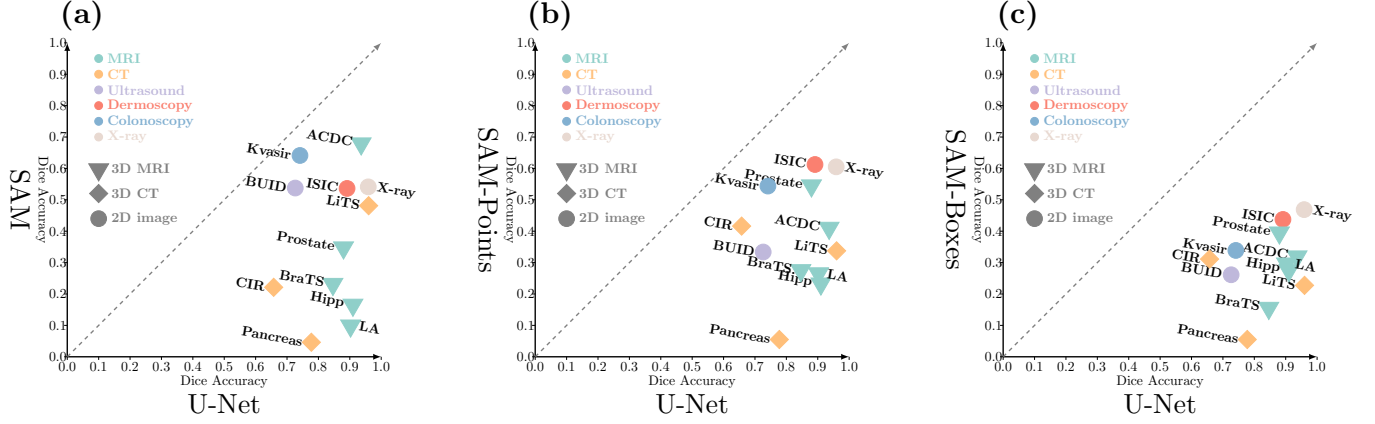


Figure 3: Scatter plot of the segmentation Dice accuracy between U-Net and SAM with different prompts ((a) auto-prompt SAM, (b) single-point prompt and (c) bounding-box prompt).

Table 1: Dice accuracies on 12 medical image segmentation datasets. U-net, U-net++, Attention U-Net, Trans U-Net, UTransNet were cross-validated in each medical image datasets. The SAM, SAM-Points and SAM-Boxes algorithms were applied directly on those 12 medical image datasets.

Data	U-Net	U-Net++	Attention U-Net	Trans U-Net	UTransNet	SAM	SAM-points	SAM-Boxes
X-ray [22]	95.83 \pm 2.64	95.63 \pm 2.80	95.78 \pm 2.69	95.74 \pm 2.87	95.56 \pm 2.86	54.12 \pm 9.88	60.52 \pm 8.39	46.85 \pm 12.62
LiTS [21]	95.95 \pm 1.64	96.12 \pm 1.49	96.04 \pm 1.60	96.02 \pm 1.44	95.57 \pm 1.70	48.15 \pm 7.90	33.72 \pm 6.58	22.76 \pm 16.09
ACDC [8]	93.60 \pm 3.10	94.19 \pm 2.97	93.59 \pm 3.59	93.69 \pm 2.79	92.97 \pm 4.10	68.20 \pm 18.53	41.34 \pm 28.43	32.25 \pm 15.60
Hippo [16]	91.02 \pm 2.28	91.09 \pm 2.42	91.06 \pm 2.33	91.02 \pm 2.39	90.97 \pm 2.38	16.83 \pm 4.04	23.68 \pm 3.57	27.86 \pm 6.25
ISIC [18], [19]	89.18 \pm 11.94	89.02 \pm 12.55	89.12 \pm 12.46	89.56 \pm 12.71	88.92 \pm 13.04	53.67 \pm 29.36	61.25 \pm 28.17	43.72 \pm 27.63
Prostate [15], [16]	88.06 \pm 3.45	88.49 \pm 3.49	88.40 \pm 3.42	87.96 \pm 3.54	87.02 \pm 3.69	35.15 \pm 20.16	54.86 \pm 22.10	39.92 \pm 7.27
LA [20]	90.29 \pm 4.05	90.85 \pm 4.09	90.84 \pm 3.42	90.83 \pm 3.45	88.80 \pm 5.78	10.28 \pm 6.85	26.88 \pm 12.33	29.98 \pm 6.08
BraTS [9], [10], [11]	84.62 \pm 9.80	85.06 \pm 9.59	84.37 \pm 10.13	85.04 \pm 9.37	84.33 \pm 9.55	23.49 \pm 8.39	27.87 \pm 10.97	15.86 \pm 15.56
Pancreas [15], [16]	77.75 \pm 7.85	78.08 \pm 7.82	78.81 \pm 7.62	78.34 \pm 7.67	73.71 \pm 9.09	4.64 \pm 1.46	5.45 \pm 2.16	5.47 \pm 4.96
BUID [12]	72.57 \pm 28.51	73.76 \pm 28.03	72.12 \pm 28.98	76.08 \pm 25.44	73.23 \pm 27.97	53.76 \pm 33.22	33.40 \pm 32.01	26.06 \pm 25.38
Kvasir [14]	74.14 \pm 26.72	75.91 \pm 25.82	72.71 \pm 28.58	77.12 \pm 22.65	73.53 \pm 27.13	64.17 \pm 28.50	54.35 \pm 30.97	33.86 \pm 29.33
CIR [13]	65.76 \pm 23.84	65.19 \pm 24.35	63.73 \pm 25.78	67.33 \pm 22.09	65.10 \pm 23.77	22.11 \pm 27.39	41.67 \pm 30.80	31.07 \pm 24.73

(SAM-Points): using the center of the ground-truth mask as the point prompt. (II) Bounding-box prompt setting (SAM-Boxes): we compute the bounding box for SAM around the ground-truth mask with a dilation of 20 pixels.

For deep learning algorithms commonly used for medical image segmentation, we trained them on 80% of the data in a dataset and tested on 20% of the data in the same dataset. For 3D images, we extract 2D slices for training and testing.

3 RESULTS

Fig. 2 and Table 1 shows the Dice accuracy of different models over 12 datasets. The main observation is that segmentation models trained directly on medical images (U-Net, U-Net++, Attention U-Net, Trans U-Net, UTransNet) provide higher Dice scores than SAM model on all 12 datasets. The 5 Deep learning algorithms widely used for medical image segmentations obtained similar Dice accuracies in each dataset. The ranking of the 3 SAM variations was not consistent across datasets. But in general, the Dice by SAM variations was often 0.1-0.5, and sometimes even 0.6-0.7 lower than the Dice accuracies by those 5 commonly used deep learning algorithms for medical image segmentation.

Fig. 3 shows the scatter plot of the Dice accuracy between U-Net and 3 SAM variations in 3 panels. It shows that SAM provides higher Dice accuracy on the 2D images from

Kvasir, BUID, ISIC and X-ray, especially by the SAM with auto-prompt [5]. The main reason might be that the SAM is trained on 2D images thus it has a good generalization to 2D medical images.

4 CONCLUSION

In this report, we conducted a comparison study of SAM's performance compared to other segmentation networks for medical image segmentation on 12 different datasets. The results show that SAM without training on medical images, has limited generalization ability on various medical images. Further studies or medical specific SAM may be expected in the future to improve the zero-shot medical image segmentation.

REFERENCES

- [1] O. Ronneberger, P. Fischer, and T. Brox, "U-net: Convolutional networks for biomedical image segmentation," in *Medical Image Computing and Computer-Assisted Intervention—MICCAI 2015: 18th International Conference, Munich, Germany, October 5-9, 2015, Proceedings, Part III* 18. Springer, 2015, pp. 234–241.
- [2] J. Schlemper, O. Oktay, M. Schaap, M. Heinrich, B. Kainz, B. Glocker, and D. Rueckert, "Attention gated networks: Learning to leverage salient regions in medical images," *Medical image analysis*, vol. 53, pp. 197–207, 2019.
- [3] Z. Zhou, M. M. R. Siddiquee, N. Tajbakhsh, and J. Liang, "Unet++: Redesigning skip connections to exploit multiscale features in image segmentation," *IEEE transactions on medical imaging*, vol. 39, no. 6, pp. 1856–1867, 2019.

- [4] S. He, R. Bao, P. E. Grant, and Y. Ou, "U-netmer: U-net meets transformer for medical image segmentation," *arXiv preprint arXiv:2304.01401*, 2023.
- [5] A. Kirillov, E. Mintun, N. Ravi, H. Mao, C. Rolland, L. Gustafson, T. Xiao, S. Whitehead, A. C. Berg, W.-Y. Lo *et al.*, "Segment anything," *arXiv preprint arXiv:2304.02643*, 2023.
- [6] H. Wang, P. Cao, J. Wang, and O. R. Zaiane, "Uctransnet: rethinking the skip connections in u-net from a channel-wise perspective with transformer," in *Proceedings of the AAAI conference on artificial intelligence*, vol. 36, no. 3, 2022, pp. 2441–2449.
- [7] J. Chen, Y. Lu, Q. Yu, X. Luo, E. Adeli, Y. Wang, L. Lu, A. L. Yuille, and Y. Zhou, "Transunet: Transformers make strong encoders for medical image segmentation," *arXiv preprint arXiv:2102.04306*, 2021.
- [8] O. Bernard, A. Lalande, C. Zotti, F. Cervenansky, X. Yang, P.-A. Heng, I. Cetin, K. Lekadir, O. Camara, M. A. G. Ballester *et al.*, "Deep learning techniques for automatic mri cardiac multi-structures segmentation and diagnosis: is the problem solved?" *IEEE transactions on medical imaging*, vol. 37, no. 11, pp. 2514–2525, 2018.
- [9] B. H. Menze, A. Jakab, S. Bauer, J. Kalpathy-Cramer, K. Farahani, J. Kirby, Y. Burren, N. Porz, J. Slotboom, R. Wiest *et al.*, "The multimodal brain tumor image segmentation benchmark (BRATS)," *IEEE transactions on medical imaging*, vol. 34, no. 10, pp. 1993–2024, 2014.
- [10] S. Bakas, H. Akbari, A. Sotiras, M. Bilello, M. Rozycki, J. S. Kirby, J. B. Freymann, K. Farahani, and C. Davatzikos, "Advancing the cancer genome atlas glioma mri collections with expert segmentation labels and radiomic features," *Scientific data*, vol. 4, no. 1, pp. 1–13, 2017.
- [11] S. Bakas, M. Reyes, A. Jakab, S. Bauer, M. Rempfler, A. Crimi, R. T. Shinohara, C. Berger, S. M. Ha, M. Rozycki *et al.*, "Identifying the best machine learning algorithms for brain tumor segmentation, progression assessment, and overall survival prediction in the BRATS challenge," *arXiv preprint arXiv:1811.02629*, 2018.
- [12] W. Al-Dhabyani, M. Goma, H. Khaled, and A. Fahmy, "Dataset of breast ultrasound images," *Data in brief*, vol. 28, p. 104863, 2020.
- [13] W. Choi, N. Dahiya, and S. Nadeem, "CIRDataset: A large-scale dataset for clinically-interpretable lung nodule radiomics and malignancy prediction," in *International Conference on Medical Image Computing and Computer-Assisted Intervention*. Springer, 2022, pp. 13–22.
- [14] D. Jha, P. H. Smedsrud, M. A. Riegler, P. Halvorsen, T. d. Lange, D. Johansen, and H. D. Johansen, "Kvasir-seg: A segmented polyp dataset," in *International Conference on Multimedia Modeling*. Springer, 2020, pp. 451–462.
- [15] M. A. Attiyeh, J. Chakraborty, A. Doussot, L. Langdon-Embry, S. Mainarich, M. Gönen, V. P. Balachandran, M. I. D'Angelica, R. P. DeMatteo, W. R. Jarnagin *et al.*, "Survival prediction in pancreatic ductal adenocarcinoma by quantitative computed tomography image analysis," *Annals of surgical oncology*, vol. 25, no. 4, pp. 1034–1042, 2018.
- [16] M. Antonelli, A. Reinke, S. Bakas, K. Farahani, A. Kopp-Schneider, B. A. Landman, G. Litjens, B. Menze, O. Ronneberger, R. M. Summers *et al.*, "The medical segmentation decathlon," *Nature communications*, vol. 13, no. 1, pp. 1–13, 2022.
- [17] Q. Liu, Q. Dou, L. Yu, and P. A. Heng, "MS-Net: multi-site network for improving prostate segmentation with heterogeneous mri data," *IEEE transactions on medical imaging*, vol. 39, no. 9, pp. 2713–2724, 2020.
- [18] N. Codella, V. Rotemberg, P. Tschandl, M. E. Celebi, S. Dusza, D. Gutman, B. Helba, A. Kalloo, K. Liopyris, M. Marchetti *et al.*, "Skin lesion analysis toward melanoma detection 2018: A challenge hosted by the international skin imaging collaboration (isic)," *arXiv preprint arXiv:1902.03368*, 2019.
- [19] P. Tschandl, C. Rosendahl, and H. Kittler, "The ham10000 dataset, a large collection of multi-source dermatoscopic images of common pigmented skin lesions," *Scientific data*, vol. 5, no. 1, pp. 1–9, 2018.
- [20] Z. Xiong, Q. Xia, Z. Hu, N. Huang, C. Bian, Y. Zheng, S. Vesal, N. Ravikumar, A. Maier, X. Yang *et al.*, "A global benchmark of algorithms for segmenting the left atrium from late gadolinium-enhanced cardiac magnetic resonance imaging," *Medical image analysis*, vol. 67, p. 101832, 2021.
- [21] P. Bilic, P. Christ, H. B. Li, E. Vorontsov, A. Ben-Cohen, G. Kaissis, A. Szeskin, C. Jacobs, G. E. H. Mamani, G. Chartrand *et al.*, "The liver tumor segmentation benchmark (LiTS)," *Medical Image Analysis*, vol. 84, p. 102680, 2023.
- [22] S. Jaeger, S. Candemir, S. Antani, Y.-X. J. Wang, P.-X. Lu, and G. Thoma, "Two public chest x-ray datasets for computer-aided screening of pulmonary diseases," *Quantitative imaging in medicine and surgery*, vol. 4, no. 6, p. 475, 2014.